



HAL
open science

Metalloenzyme-Mediated Thiol-Yne Addition Towards Photoisomerizable Fluorescent Dyes

Alexis Lossouarn, Chloé Puteaux, Laetitia Bailly, Vincent Tognetti, Laurent Joubert, Pierre-yves Renard, Cyrille Sabot

► **To cite this version:**

Alexis Lossouarn, Chloé Puteaux, Laetitia Bailly, Vincent Tognetti, Laurent Joubert, et al.. Metalloenzyme-Mediated Thiol-Yne Addition Towards Photoisomerizable Fluorescent Dyes. Chemistry - A European Journal, In press, 10.1002/chem.202202180 . hal-03808088

HAL Id: hal-03808088

<https://normandie-univ.hal.science/hal-03808088>

Submitted on 25 Oct 2022

HAL is a multi-disciplinary open access archive for the deposit and dissemination of scientific research documents, whether they are published or not. The documents may come from teaching and research institutions in France or abroad, or from public or private research centers.

L'archive ouverte pluridisciplinaire **HAL**, est destinée au dépôt et à la diffusion de documents scientifiques de niveau recherche, publiés ou non, émanant des établissements d'enseignement et de recherche français ou étrangers, des laboratoires publics ou privés.

Metalloenzyme-Mediated Thiol-Yne Addition towards Photoisomerizable Fluorescent Dyes

Alexis Lossouarn[†],^[a] Chloé Puteaux[†],^[a] Laetitia Bailly,^[a] Vincent Tognetti,^{*[a]} Laurent Joubert,^[a] Pierre-Yves Renard,^[a] and Cyrille Sabot^{*[a]}

[a] Dr. A. Lossouarn, C. Puteaux, L. Bailly, Prof. L. Joubert, Dr. V. Tognetti, Prof. P.-Y. Renard, Dr. C. Sabot
Normandie Univ, CNRS, UNIROUEN, INSA Rouen, COBRA (UMR 6014), Rouen 76000, France
E-mail: vincent.tognetti@univ-rouen.fr, cyrille.sabot@univ-rouen.fr (homepage : <https://www.lab-cobra.fr/>)

[*] [These two persons have equally participated to this work.](#)

Abstract: *Proteins are able to irreversibly assemble biologically active ligands from building blocks bearing complementary reactive functions due their spatial proximity, through a kinetic target-guided synthetic process (also named in situ click chemistry). Although linkages thus formed are mostly passive, some of them have shown to significantly contribute to the protein binding through for instance hydrogen bonding and stacking interactions. Biocompatible reactions and click chemistry are a formidable source of inspiration for developing such new protein-directed ligations. In this study, we report a proximity-induced thiol-yne synthesis of carbonic anhydrase inhibitors. Not only this example widens the arsenal of Kinetic target-guided synthesis (KTGS) eligible reactions, but the obtained product displayed unsuspected photophysical properties. The corresponding vinyl sulfide linkage conjugated to a coumarin core proved to be engaged in a monodirectional Z to E photoisomerization process. Further investigations guided by theoretical calculations showed that fine-tuning of the nature of the substituents on the coumarin moiety allows to obtain a bidirectional photochemical process, thus discovering a new photoswitching moiety, displaying moreover fluorescence properties. Due to the spectral tunability of coumarin derivatives, this work should open new opportunities for the design of vinyl sulfide-based photoswitch systems with modular photophysical properties.*

Introduction

Drug discovery is repeatedly facing the challenge of finding new biological targets, pharmacophores, or elucidating novel mechanisms of action, in a time- and cost-effective manner.^[1] This interdisciplinary field of research benefits from constant innovations in biophysics (X-ray crystallography, NMR & surface plasmon resonance (SPR) spectroscopy, isothermal titration calorimetry (ITC)),^[2] in computing technologies, including machine learning processes opening new frontiers to yet underexploited scaffolds,^[3] in high-throughput screening with wide range of sophisticated assays and automated evaluation of large numbers of chemical/biological compounds.^[4] Important advances in drug design have also been achieved with contributions from chemistry, in particular with the diversity-oriented synthesis which generates structural diversity in an efficient manner,^[5] and with the kinetic target-guided synthesis (KTGS) strategy which allows the synthesis and the identification of potent pharmacophores in a single step process.^[6]

In KTGS, the biological target is able to assemble its own ligands by linking together two fragments bearing complementary reactive chemical functions due to their spatial proximity. This technology enabled the discovery and/or optimisation of bioactive molecules with more than 50 examples, covering 10 different therapeutic areas.^[6e] Importantly, this method allowed the identification of unknown protein conformations,^[7] or previously hidden binding pockets.^[8] A handful of chemical ligation strategies have been reported to form a covalent bond between recruited fragments within the binding pocket of biological targets, among which the alkyne-azide 1,3-dipolar cycloaddition reaction leading to the formation of 1,4- or 1,5-triazole linkages has been used predominantly.^[9] The triazole ring system has shown to offer a substantial additional and beneficial binding contribution with π - π stacking and hydrogen-bonding interactions.^[7] More recently, Rademann and co-workers also highlighted a superadditive fragment combination through a protein-induced Mannich ligation.^[10] Recent developments in protein-templated chemistry also include the amidation from activated carboxylic acids and amines,^[11] the Knoevenagel reaction,^[12] and the Ugi four-component reaction.^[13]

Other ligation strategies can be implemented by drawing inspiration from biocompatible and click chemistry portfolio reactions used in bioorthogonal bioconjugate processes, by tuning their kinetics to meet the requirements for use in KTGS strategies.^[14] This can be achieved by structural modifications of the reactive partners in order to decrease their reactivity^[15] or by removing the catalyst such as in the alkyne-azide click chemistry.^[9] In this context, thiol-yne^[16] click chemistry would offer attractive features such as the small size of the reactive moieties, the accessibility and apparent robustness of the alkyne group, and the requirement of additives or catalysts such as amines,^[17] transition metals^[18] or photoinitiators^[19] to promote the reaction. This strategy has found key roles in polymer chemistry, biomaterials synthesis and surface modifications.^[20] Importantly, Ovaal^[21] and Mootz^[22] have independently used alkynes as latent electrophiles for the design of covalent inhibitors upon their reaction with thiol group of enzymes, which contain an active site cysteine (Figure 1A).

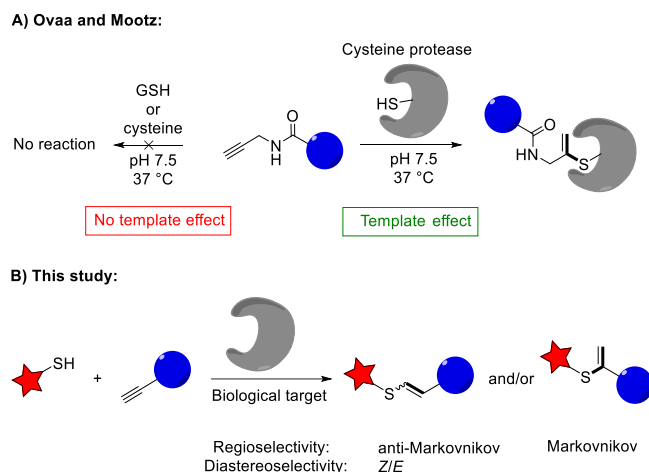


Figure 1. Thiol-yne reaction used for A) covalent cysteine protease inhibition, B) proteins-directed inhibitors synthesis (KTGS).

These important results show that the thiol-yne reaction can be triggered by a proximity effect (*i.e.*, without any other external activation). This and other considerations discussed above prompted us to investigate this reaction as a new plausible ligation tool for the protein-directed synthesis of ligands (Figure 1B). In this study, we illustrate the potential of the thiol-yne addition in KTGS through the implementation of this click reaction to a model metalloenzyme whose specific inhibition is of interest for the treatment of several diseases.

Results and Discussion

Carbonic anhydrase II (CA-II) selected as the model protein to evaluate the potential of thiol-yne reaction in KTGS is a zinc-containing metalloenzyme that catalyses the reversible hydration of carbon dioxide (CO_2) to generate bicarbonate (HCO_3^-) and a proton (H^+), through a metal hydroxide nucleophilic species. The zinc ion is located at the bottom of a 16 Å deep canonical active site, where it is tetrahedrally coordinated by three imidazole groups of His residues and by one hydroxide ion. CA is ubiquitous in numerous tissues, and involved in a variety of physiological processes, including pH regulation, gas exchange, ion transport, bone resorption, fatty acid metabolism. Inhibitors of CAs are clinically used for the treatment of glaucoma, oedema, altitude sickness, and epilepsy.^[23] Up-regulation or overexpression of CAs may be associated with physiological disorders such as tumours, and neurodegenerative pathologies such as Alzheimer disease.^[24]

Sulfonamides are an important class of CA inhibitors due to their effective binding to the zinc(II) ion, thereby preventing the binding of the endogenous CO_2 and H_2O substrates.^[25] Accordingly, in this study, a readily accessible α -mercaptotosylamide **1a** playing the role of anchor was incubated with a series of aliphatic- **2a-d** or aromatic alkynes **2e-h** as binary mixtures, in parallel of negative controls without enzyme (Figure 2). Alternatively, the alkyne-bearing sulfonamide 4-ethynylbenzenesulfonamide **2f** was incubated with heteroaromatic thiols **1b**, **1c** or the thiobenzyl alcohol **1d**. The crude reaction mixtures were analysed by LC-MS/MS or LC-HRMS and compared with products obtained from chemical synthesis.

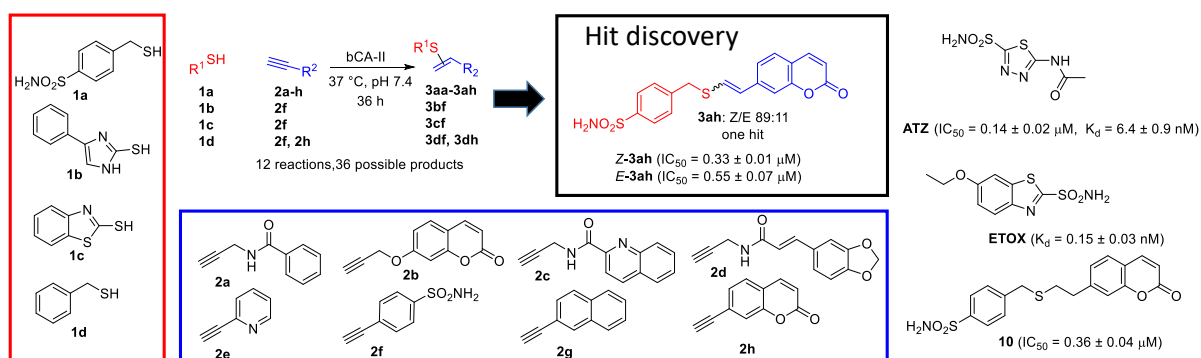


Figure 2. Library of KTGS experiments between thiols (60 μM), alkynes (400 μM), bCA-II (30 μM).

From this study, a ~2- to 10-fold acceleration (depending on the protein reference and batch, see SI section 7, S45-50) of the thiol-yne addition reaction between **1a** and **2h** leading to the vinyl sulfide **3ah** (as a mixture of diastereoisomers *Z/E*: 89:11) was observed, as compared with the control experiments carried out in the absence of *bCA*-II. No trace of the Markovnikov thiol-yne product (Figure 1B) was detected, nor in the untemplated reaction. Of note, the formation of **3ah**, although in the subnanomolar range, was significantly affected by the presence of acetazolamide **ATZ** or ethoxazolamide **ETOX** (3.3 equivalents relative to the active-site binder **1a**), two highly effective commercially available active-site *bCA*-II submicromolar inhibitors. Moreover, the reaction carried out between the non-zinc coordinating analogue **1d** of **1a**, and **2h** was not accelerated in the presence of *bCA*-II. Together, these results confirmed that templated reaction occurred in the active site of the *bCA*-II and not in another hidden pocket or binding site. Then, the biological activity of templated products *Z-3ah* and *E-3ah* was evaluated through 4-nitrophenyl acetate hydrolysis assays (see SI section 9, S62)^[26] by measuring their half maximal inhibitory concentration (IC_{50}), which was found to be 0.33 ± 0.01 and 0.55 ± 0.07 μ M, respectively, while acetazolamide **ATZ**, has an IC_{50} value of 0.14 ± 0.02 μ M (Figure 2). A flexible thioether analogue **10** was prepared in order to investigate the impact of the rigidity of the vinyl sulfide linkage of **3ah** on the biological activity, and its activity (0.36 ± 0.07 μ M) was found to be in the range of that of the most active *Z-3ah*. The stability of the vinyl sulfide linkage of **3ah** was investigated in the presence of biothiols (N-acetyl cysteine, glutathione), as well as in human blood plasma (HBP) after a few days of incubation at 37 °C. Neither thiol release nor degradation was noticed, which confirms the stability of **3ah** and the irreversibility of the reaction under physiological conditions. In contrast, the thioether analogue **10** was partially oxidized (~5%) into the corresponding sulfoxide after incubation in HBP at 37 °C for 3 days (see SI section 8.1 S51-61).

While the starting 7-ethynylcoumarin was not emissive in PBS,^[27] both **3ah** isomers displayed fluorescence properties, with very similar absorption and emission spectra (Figure 3A and 3B). They exhibited a relatively high emission wavelength (510 nm) and an unusual large Stokes shift (155 nm) for low molecular-weight coumarin derivatives.^[28] However, their fluorescence quantum yields are significantly different with 0.16 and 0.52 for *Z-3ah* and *E-3ah*, respectively in PBS pH 7.4. Whilst the absorption spectrum displays a minor change with decreasing polarity of the solvent, a hypsochromic shift (up to 88 nm) of the fluorescence emission spectrum was observed (Figure 3C and see SI section 10.5 S72-74).

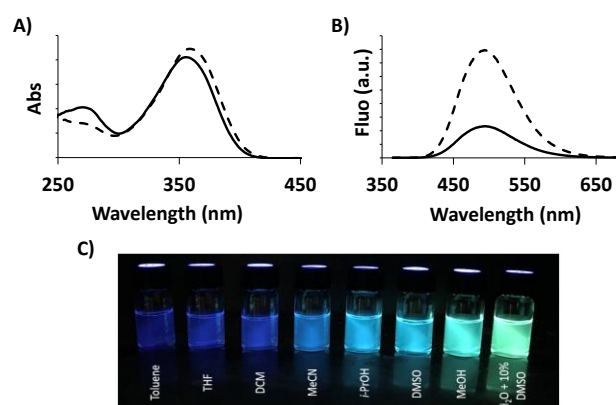


Figure 3. Photophysical properties of vinyl sulfide coumarin **3ah**. A) Relative absorption of *Z-3ah* (—) and *E-3ah* (---) in H₂O/DMSO 1:1 (v/v) at 25 °C; B) Relative emission of *Z-3ah* (—) and *E-3ah* (---) λ_{ex} 350 nm in H₂O/DMSO 1:1 (v/v) at 25 °C; C) Photograph of *E-3ah* (10 μ M) in different solvents under UV light (λ_{ex} = 365 nm).

These unusual optical features were found to be particularly suitable for their use in the intrinsic Förster Resonance Energy Transfer (iFRET) technique,^[29] which could further support the existence of specific protein-ligand interactions between *CA*-II and the vinyl sulfide inhibitor **3ah**. In fact, the iFRET approach uses a FRET mechanism between endogenous tryptophan (Trp) residues ($\lambda_{abs} \sim 280$ nm, $\lambda_{em} \sim 310$ -350 nm) that are in close proximity to fluorescent ligands bound in the active site of target proteins, which act as donor (D) and acceptor (A), respectively (Figure 4A). However, the limited Stokes shift of reported probes used in such iFRET experiments such as 1-naphthylamine or 7-hydroxycoumarin dyes are subject to self-absorption,^[30] or display low sensitivity such as the dansyl moiety,^[31] which decreases the FRET efficiency. Accordingly, the use of vinyl sulfide-based coumarin as a new acceptor in Trp-FRET was examined in order to address these issues. First, excitation of Trp residues at 280 nm of a solution of *bCA*-II (2 μ M) in PBS (pH 7.4) led to an emission band centred at 336 nm. This emission peak significantly decreased in the presence of *Z-3ah* (2 or 4 equiv.), evidenced by an iFRET efficiency *E* of 86%, which was determined from the equation $E = 1 - I_{DA}/I_D$ (where I_{DA} and I_D are the intensities of the donor D in the presence or in the absence of the acceptor A, respectively) (Figure 4B).^[29]

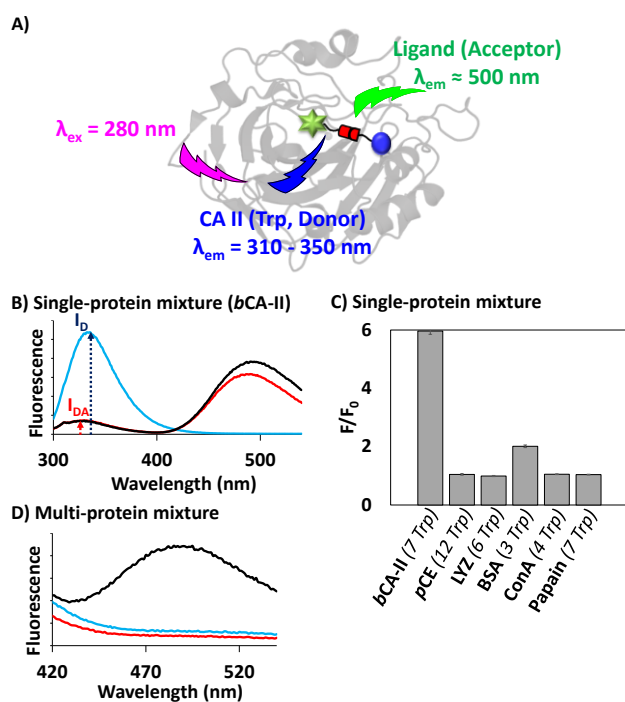


Figure 4. Analysis of Trp-FRET experiments. A) iFRET principle; B) Fluorescence emission spectra of a solution of *bCA-II* (2 μM) in the absence (in blue), or in the presence of **Z-3ah** (2 μM in red, 4 μM in black), upon an excitation at 280 nm, in PB pH 7.4; C) Relative fluorescence intensity observed at 495 nm of a solution of **Z-3ah** (1 μM) in the presence of various proteins (2.5 μM), upon an excitation at 280 nm, in PB pH 7.4; and D) fluorescence emission of **Z-3ah** (1 μM) in a solution containing five **Z-3ah** non-target proteins (PCE, LYZ, BSA, ConA, papain, 2.5 μM each) in the absence (in blue) or in the presence of *bCA-II* (2.5 μM , without **ATZ** in black; or with 100 μM **ATZ** in red), upon an excitation at 280 nm, in PB pH 7.4.

Moreover, **Z-3ah** undergoes a 15 nm hypsochromic shift in the emission spectrum upon binding to *bCA-II* (from 510 to 495 nm), which, together with **Z-3ah** solvatochromic character is consistent with a hydrophobic environment surrounding the fluorophore in the CA active site. Next, as negative controls, **Z-3ah** was incubated with different non-target proteins as binary mixtures, including porcine liver esterase (*pLE*), lysozyme (LYZ), bovine serum albumin (BSA), concanavalin A (ConA) and papain (Figure 4C). None of them led to a significant fluorescence enhancement in the probe region compared with the probe alone, a result which also indicates the probe's specificity for the *bCA-II* binding site. Only BSA displayed a 2-fold increase in fluorescence intensity, which could be associated to non-specific probe-protein interactions. This is often observed with this major small molecules binding protein, which size and collection of non-specific binding sites are used to transport a wide range of fluorophores or drug like small molecules and even to solubilize dye aggregates.^[32] Finally, the fluorescence response of a solution of **Z-3ah** (1 μM) towards a mixture of these five non-target proteins (2.5 μM each) was investigated. No significant fluorescence was observed in the 500 nm region (in blue, Figure 4D) whereas the fluorescence intensity of probe **Z-3ah** showed a 10-fold increase in this spectral region when *bCA-II* (2.5 μM) was present in the protein mixture (in black, Figure 4D). Of note, in the presence of **ATZ** (100 μM), no more significant iFRET signal was detected (in red, Figure 4D).

During preliminary studies, we also observed an *E* to *Z* isomerization of the vinyl sulfide double bond of **3ah** in aqueous solution upon exposure to ambient light, at room temperature. This photophysical behaviour caught our attention and was further investigated, as only few chemical scaffolds have been reported to undergo such catalyst-free reversible photoisomerization despite the increasing importance of photoswitch systems for the fine control of materials and biological systems properties^[33] with applications in drug delivery,^[34] bio-imaging,^[35] or in the development of hydrogels.^[36] Major classes of photoswitchable molecules include azobenzenes,^[37] stilbenes,^[38] diarylethenes,^[39] or spiropyranes,^[40] and emerging systems such as hydrazones,^[41] iminothioindoxyls.^[42]

Among them, azobenzenes received considerable attention due to their straightforward synthetic access and good photo-fatigue resistance, although substantial efforts have been devoted to overcome shortcomings such as short thermal half-lives of *Z*-isomers (metastability), and incomplete reverse *Z* to *E* photoisomerizations due an overlap of the $n \rightarrow \pi^*$ bands of *E* and *Z* isomers. In this present study, the conversion of the *Z*-isomer into its *E*-form was first confirmed by ¹H NMR spectroscopy studies upon the exposure of an isomeric mixture of **3ah** (*Z/E* 70:30) to ambient light source, which shifted the ratio in favour of the *E*-isomer (45:55) (dotted curve, Figure 5A). Starting from the pure *Z* isomer, a photostationary state (PSS) containing 82% of the *E* isomer was rapidly reached in aqueous system, under 365 nm LED spotlight irradiation (continuous curve, Figure 5B). This PSS isomeric composition was confirmed by irradiating the pure *E* isomer, which underwent isomerization reaching the same equilibrium state (Figure 5B). Then, the photostationary

equilibrium was determined upon the irradiation of **Z-3ah** with blue visible LEDs of different wavelengths (380, 405, 450 nm). In all these studies, the *E* isomer was obtained preferentially, albeit with different proportions (PSS_{380 nm} = 77%; PSS_{405 nm} = 73%; PSS_{450 nm} = 64%). A monochromatic excitation at 300 nm, or 450 nm by using a xenon lamp coupled with a monochromator did not increase the proportion of *Z* isomer. From these results, it was, however, anticipated that reversible photoisomerization would occur but with a low amplitude as shown in Figure 5C, upon alternating the irradiation wavelength between 365 and 450 nm. The *Z* isomer has shown to be highly stable in the dark and can be kept for several months at room temperature without noticeable isomerization. Thermal conditions (80 °C for 2h) did not enable *Z* to *E* isomerization, which was also confirmed by density functional theory (DFT) calculations since the ground state activation barrier for this step was found to be equal to 61 kcal mol⁻¹ in pure implicit DMSO in terms of standard Gibbs energy with respect to *E* diastereoisomer, which is 1.6 kcal mol⁻¹ more stable than the *Z* diastereoisomer (see SI section 13.6, S167).

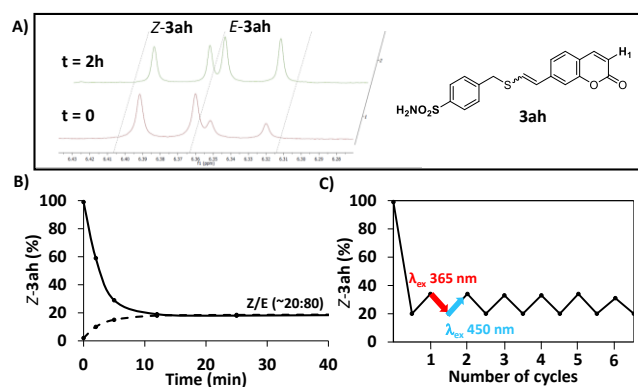


Figure 5. Photoisomerization studies of **3ah**. A) Partial ¹H NMR (DMSO-d₆/D₂O 75:25, 300 MHz, 298 K) showing the lactone region (H₁) of **3ah** at t=0 (Z/E, 70:30) and after 2h (Z/E, 45:55) irradiation under ambient light source; B) Time-course of photoisomerization of **Z-3ah** (solid line) and **E-3ah** (dotted line) upon irradiation at 365 nm (LED spotlight) determined by RP-HPLC (detection at 350 nm); C) Photofatigue-resistance of **3ah** upon alternating irradiation at 365 nm and 450 nm (LED spotlight) determined by RP-HPLC (detection at 350 nm).

Although vinyl sulfide coumarin **3ah** still constitutes a rare example of fluorescent molecules with a photoswitchable character,^[41, 43] the low *E* to *Z* photoconversion prevents any important applications in this field. Therefore, as a natural extension of these studies, we questioned whether further optimization, guided by theoretical studies, would be possible. Indeed, the strong overlap of the absorption spectra of both isomers, prevents *Z* enriched PSS. This issue may be circumvented by the introduction of specific chemical functions (electron withdrawing or electron donating groups) on the coumarin ring at positions 3, 4, that are known to significantly alter its absorbance.^[28, 44] Besides, the introduction of chemical functions at position 6, and/or 8, that are at the *ortho*-position of the vinyl sulfide moiety, may intuitively cause a distortion of the planar *Z* isomer, thus affecting specifically its $\pi \rightarrow \pi^*$ transition.

These features can be tackled from a quantum chemistry point of view using time-dependent DFT (TD-DFT, see SI section 13.1, S108 for the computational details). To this aim, eight common substituents, representative of inductive and mesomeric electron withdrawing or -donating moieties were considered (CH₃, CF₃, CN, CO₂H, OCH₃, F, Cl, Br) and tested at each of these positions. Note that in order to understand the role of a given site, hydrogen atoms only were first considered on the three remaining positions. Besides, for the sake of simplicity, only the *s-trans* conformation of the C=C double bond linking the coumarin to the sulfide moiety was investigated, as represented in Figure 6. Due to steric hindrance, such a conformation does not actually allow accommodating the CF₃, CO₂H, Cl and Br substituents in position 6, so that the vertical absorption wavelengths (corresponding to the ground state to the first electronic excited state transition) for *Z* and *E* isomers were computed for 28 mono-substituted compounds in implicit pure DMSO solvent (coordinates and energies are collected in sections 13.2 and 13.3 in SI).

As shown in Figure 6 and in section 13.5, S166, the absorption wavelength is lower for the *Z*- than for *E* isomer in almost all cases (only 5 exceptions), and there are only two of them that feature a significant $\Delta\lambda$ difference: 35 nm for R⁶ = CN and 19 nm for R⁶ = F. Noteworthy, in both cases, the *Z* isomer is far from being planar (the C^aC^bC⁷C⁶ dihedral angle being equal to 69° and 46°, respectively). Moreover, all substitution patterns exhibiting a $\Delta\lambda$ value higher than 5 nm, involve a *Z* isomer for which \angle C^aC^bC⁷C⁶ is higher than 35°. However, this non-planarity condition, while necessary, is not sufficient

to ensure a high $\Delta\lambda$ value, as exemplified by the $R^8=\text{CO}_2\text{H}$ case for which $\angle\text{C}^a\text{C}^b\text{C}^7\text{C}^6 = 41^\circ$ and $\Delta\lambda = 1$ nm, proving that structural and electronic effects cannot be fully disentangled.

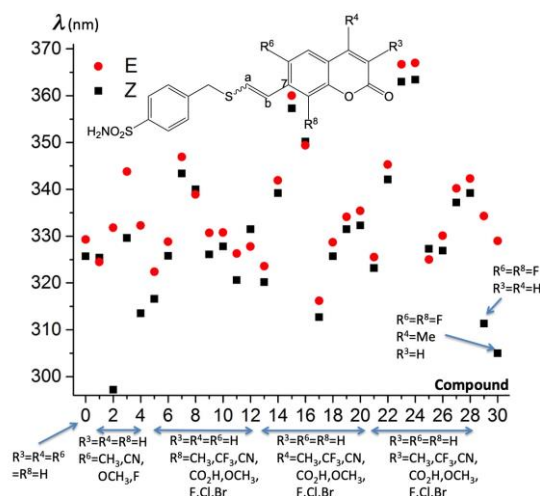


Figure 6. Calculated vertical absorption wavelengths (in nm) for the $S_0 \rightarrow S_1$ vertical electronic transition in selected molecules. CAM-B3LYP/6-31++G(d,p) level of theory, pure DMSO is treated as an implicit solvent by the IEF-PCM model.

One may also wonder whether a simple molecular orbital (MO) analysis could be used instead of this more time-consuming TD-DFT approach. As shown in section 13.4, S165, the frontier canonical Kohn-Sham MO gap, \mathcal{E}_{gap} , is nicely linearly correlated to the absorption wavelength according to $\lambda = 1.61hc/\mathcal{E}_{gap}$ with a mean absolute error equal to 3 nm. However, such an approach would be inefficient for accurate screening. Indeed, it reveals unsatisfying to predict wavelength differences and even their correct sign. For instance, for $R^8 = \text{CH}_3$, it gives $\Delta\lambda = +5$ nm, while the TD-DFT value is -6 nm. Secondly, the slope of this linear model is a little bit far from 1.0, suggesting that the electronic transition might be more complex than a simple HOMO→LUMO transition. Indeed, even if, for most systems, this mono-electronic transfer (as expected of the $\pi \rightarrow \pi^*$ type, as pictured in section 13.7, S171) represents about 85-90% of the transition, it only describes 75% and 82% of it for Z isomer with $R^6=\text{CN}$ and F respectively, which are, as previously mentioned, the most promising systems.

However, while featuring the highest $\Delta\lambda$ value, $R^6 = \text{CN}$ is subsequently disqualified by its low value for the Z absorption wavelength (297 nm), which is actually too far from the visible spectrum, precluding its practical use in a biological context. We thus turned our attention to the fluorine substitution. Interestingly, adding another fluorine atom in position 8 resulted in a non-negligible increase (compound #29 in Figure 6) of the wavelength separation, leading to $\Delta\lambda = 23$ nm. However, from a synthetic point of view, adding a methyl group in position 4 leads to a much more straightforward synthesis (see below), with a very slight increase of the $\Delta\lambda$ values (24 nm, compound #30 in Figure 6) and keeping the significant non-planarity ($\angle\text{C}^a\text{C}^b\text{C}^7\text{C}^6 = 48^\circ$, coordinates and views in section 13.8 in SI).

In order to experimentally verify this theoretical screening strategy, the synthesis of the 4-methyl-6,8-difluorocoumarin **17** (i.e. compound #29: $R^3 = R^4 = \text{H}$, $R^6 = R^8 = \text{F}$, Figure 6) was achieved in 5 steps and 33% overall yield from commercially available 2,4-difluororesorcinol, and obtained as a mixture of Z/E diastereoisomers (63:37), that were separated by RP-HPLC (see SI section 4.2, S19).

Isomers Z- and E-**17** in hand, their biological activities were determined and found to be 0.30 ± 0.05 and 0.99 ± 0.11 μM , respectively, thus demonstrating that the presence of an extra methyl group (position 3) and two fluorine atoms (position 6 and 8) did not significantly alter the biological activity of the reference compound **3-ah**. Regarding the photophysical properties of **17** (Figure 7A-B), satisfyingly, a ~ 20 nm bathochromic shift of the absorption maximum of the Z isomer (λ_{max} 337 nm) was observed with theoretical predictions (305 and 329 nm, respectively, in pure implicit DMSO – experimental values being recorded in a H₂O-DMSO mixture), proving the reliability of the computational protocol for semi-quantitative screening. Both isomers were fluorescent with emission maxima at 495 nm, and a quantum yield of 0.06 and 0.22 for Z-**17** and E-**17**, respectively.

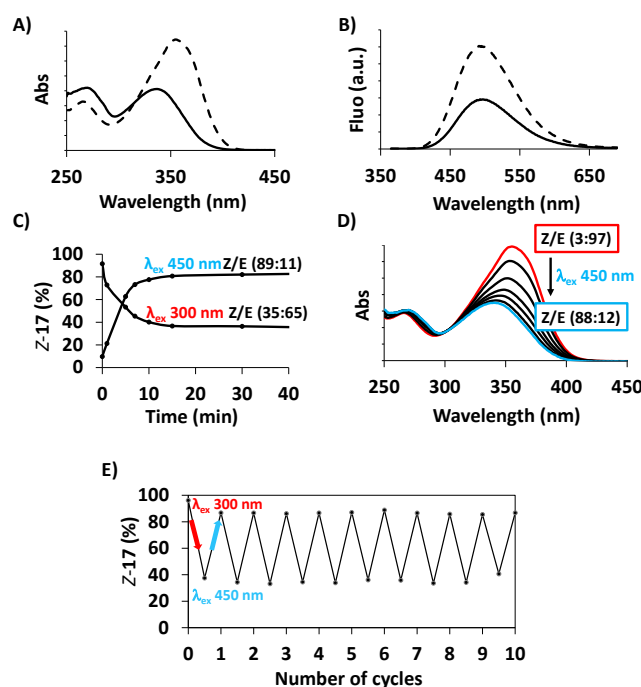


Figure 7. Photoisomerization studies of **17**. A) Relative absorption of **Z-17** (—) and **E-17** (---) in $\text{H}_2\text{O}/\text{DMSO}$ 1:1 (v/v) at 25 °C. B) Relative emission of **Z-17** (—) and **E-17** (---) λ_{exc} 350 nm in $\text{H}_2\text{O}/\text{DMSO}$ 1:1 (v/v) at 25 °C; C) Time-course of photoisomerization of **Z-17** upon irradiation at 300 nm (monochromator) and **E-3ah** upon irradiation at 450 nm (LED spotlight), determined by RP-HPLC (detection at 303 nm); D) Evolution of the absorption spectra for **E-17** (in red) under irradiation at 450 nm (LED spotlight) after 1, 3, 5, 7, 10 min. (in black), and 15 min. (in blue); E) Photofatigue-resistance of **17** upon alternating irradiation at 300 nm (monochromator) and 450 nm (LED spotlight), determined by RP-HPLC (detection at 303 nm).

Then, the composition of the PSS was investigated upon the irradiation of **17** at different wavelengths (300, 350, 400, 450 nm) with a xenon lamp coupled with a monochromator (see SI). Using light at 300 nm, **Z-17** photoswitched to generate a PSS of 65% E isomer. Conversely, **E-17** underwent a remarkable E to Z photoisomerization under irradiation at 450 nm providing the Z isomer with a PSS of 87% (Figure 7C). Noteworthy, LEDs did not provide effective Z to E isomerization (see SI section 12.8, S103-104).

TD-DFT calculations were then carried out to cast the light on the physico-chemical origin of this conversion. To this aim, vertical excitations were performed along the minimum energy reaction path (monitored by intrinsic reaction coordinate ξ) for the ground state S_0 isomerization process to approximate excited state potential energy surfaces (PESs), as depicted in Figure 8 (note that the rotation itself around the C=C double bond mainly occurs in the small [-5; 5 $\text{amu}^{1/2}\text{bohr}$] ξ range, see right vertical axis). The S_0 and second excited state S_2 energy profiles display a similar shape with a maximum around $\angle\text{HCCH} = 90^\circ$. The corresponding activation barriers from **E** isomer (which is the thermodynamically most stable one) were found respectively equal to 55 and 26 kcal mol^{-1} .

Conversely, the energy is minimal at this point for the first excited state S_1 . The PES topology corresponds with a conical intersection (CI) with the ground state, allowing a non-radiative transition between S_1 and S_0 . The photo-induced **E** \rightarrow **Z** isomerization mechanism is thus the following: (i) vertical excitation from **E** to E^* , (ii) reaching the highest local point $A1^*$, a step that requires an activation energy equal to only 11 kcal mol^{-1} (less than 0.5 eV), (iii) reaching the CI zone, (iv) non-emissive transition to S_0 , (v) vibrational structural relaxation towards either **E**- or **Z** isomer. Obviously, evaluating the rate constants and branching ratios of such steps are clearly outside the scope of this static approach, which is however able to qualitatively account for the observed isomerization process and that is fully consistent with similar mechanisms reported for stilbenes.^[45]

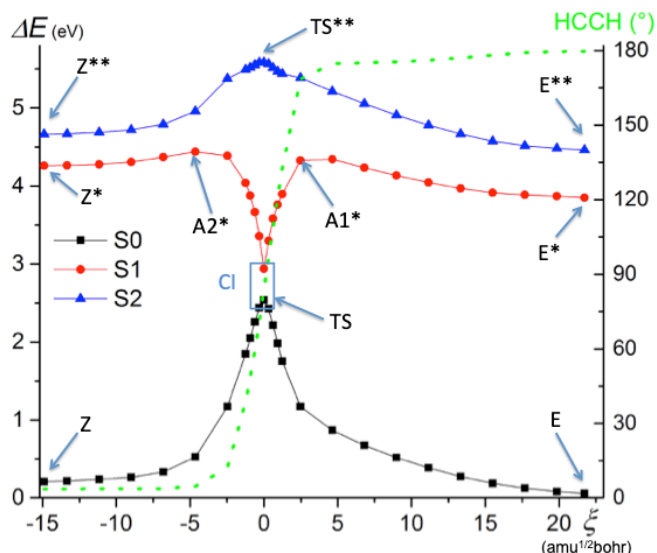


Figure 8. Calculated energy profiles (ΔE) of the three lowest electronic states for the *Z-E* isomerization process for compound **17** as a function of intrinsic reaction coordinate ξ and variation of the HCCH dihedral angle (right vertical axis). CAM-B3LYP/6-31++G(d,p) level of theory, DMSO is treated as an implicit solvent by the IEF-PCM model.

Altogether, these results demonstrate that vinyl sulfide patterns can be subject to effective bidirectional photoconversion and that in aqueous systems. The progress of the *E* to *Z* photoisomerization process was followed by recording the absorption spectra of the reaction at different times (Figure 7D). As the reaction progresses, the maximum absorption peak at 355 nm, corresponding to the $\pi \rightarrow \pi^*$ transition of the *E* isomer, decreases and shifts towards higher energy to stabilize at 337 nm corresponding to the isomeric mixture at PSS_{450 nm} (*Z/E*, 88:12). Figure 7E highlights the good photofatigue-resistance of **17** upon several photoisomerization cycles. Finally, no *Z* to *E* isomerization was observed when *Z-17* was incubated at 20 or 40 °C in the darkness for more than 50 days, which further illustrates the robustness of vinyl sulfide pattern (see SI section 12.10, S106-107).

Conclusion

This work reports (1) an unprecedented thiol-yne protein-assisted KTGS ligation on small, accessible alkyne and thiol partners, which enabled (2) the identification of a submicromolar inhibitor of *bCA-II*. It is worth noting that we identified thiol-yne reaction as a potential candidate for KTGS in a recent study evaluating tailored bioorthogonal and bioconjugate chemistry as potential source of inspiration to discover new KTGS eligible reactions.^[14] We also found (3) that the vinyl sulfide linkage, formed by the addition of thiol to alkyne groups, is an effective, yet unexplored, electron-donating group for the design of coumarin based fluorophores with large Stokes shifts, with potential applications in bio-imaging or biological target identification in complex media.

Besides, (4) this work underscored the bidirectional photoswitching behaviour of these fluorescent vinyl sulfides coumarine derivatives in aqueous systems, whose (5) spectral properties could be fine-tuned by structural modifications guided by a theoretical *in-silico* design. In this context, it was observed that the introduction of fluorine atoms in *ortho* position on the coumarin ring caused a ~20 nm splitting of *E* and *Z* isomers' $\pi \rightarrow \pi^*$ bands, which enabled effective bidirectional photoconversion of thermally bistable isomers. The *Z* to *E* photoisomerization required UV light, which may temper the impact of this approach for some biological applications. However, the red shift of spectral bands of coumarins by modifications of the lactone ring are well documented,^[28, 44] moreover we also noticed from theoretical considerations that such modifications should not impact the maximum absorption wavelengths difference between the *E* and *Z* isomers. Thus, as a direct perspective, the development of fluorescent vinyl sulfides conjugated to coumarin rings capable of photoswitching exclusively under visible light excitation could be envisioned.

Experimental Section

General remark: Unless otherwise stated, all chemicals were used as received from commercial sources without further purification. *bCA-II* was purchased from Merck-Sigma-Aldrich (reference C2624, lyophilized powder >95% SDS-PAGE, specific activity $\geq 3,500$ W-A units/mg protein; and reference C2522, lyophilized powder, $\geq 3,000$ W-A units/mg protein) and was stored at -20 °C. Triethylamine and diisopropylethylamine (DIPEA) were distilled over KOH and CaH₂, respectively. Solvents, unless otherwise stated, were purchased in reagent grade or HPLC grade and used as received. Dry solvents were obtained following standard procedures: N,N-dimethylformamide (DMF) was purchased as dry solvent from Fisher Scientific and stored over 3 Å molecular sieves; Tetrahydrofuran (THF) was distilled over

sodium/benzophenone; Dichloromethane (DCM), acetonitrile (ACN), toluene and diethylether were obtained from MB SPS-800 apparatus from MBRAUN ; isopropanol, methanol and acetone were stored over molecular sieves (3 Å or 4 Å according to the solvent) prior to use. For non-aqueous reactions, flasks were dried by heating with a heat gun under vacuum. All reactions were monitored by thin layer chromatography (TLC) and/or RP-HPLC. TLC were carried out on Merck DC Kieselgel 60 F-254 aluminum sheets. Visualization of spots was performed under a UV lamp at $\lambda = 254$ or 365 nm, and/or staining with a KMnO_4 solution/ K_2CO_3 + 5% NaOH, developed with heat. Flash column chromatography purifications were performed manually on silica gel (40–63 μM) under pressurized air flow. Aqueous buffers such as tris(hydroxymethyl)aminomethane (Tris) (pH 7.6, 0.05 M), phosphate buffer salin (PBS) (pH 7.4, 0.1 M) or phosphate buffer (PB) (pH 7.4, 0.25 M) and aq. mobile phases for HPLC were prepared using water that was purified with a Milli-Q system (purified to 18.2 M Ω cm) and were stored at 4 °C. Formic acid (FA) for mobile phases was purchased in HPLC grade (Fisher Scientific or Acros Organics) and stored at 4 °C. For LC-MS analyses, ultrapure water (Alfa Aesar, LC-MS quality) was employed for the preparation of mobile phases.

Instruments: ^1H , ^{19}F and ^{13}C NMR spectra were recorded on 300 MHz Bruker FT-NMR machine operating at ambient probe temperature. High Resolution Mass spectrometry (HRMS) for compounds characterization was performed with a Waters Micro-mass LCT Premier XE® equipped with an orthogonal acceleration time-of-flight and an electrospray source in positive or negative mode. Infrared spectra were recorded with a universal ATR accessory on a Perkin-Elmer Spectrum One FT-IR spectrum 100 spectrometer. Melting points were recorded on a LEICA VMHB Kofler system at atmospheric pressure and without correction. UV-Vis spectroscopy was performed on an Agilent Cary 60 UV-Vis® at 20 or 25 °C. Fluorescence spectroscopic studies (emission/excitation spectra) were performed on a Horiba Scientific Fluorolog® spectrophotometer, equipped with a Hamamatsu photomultiplier tube R13456 and a xenon 450 W illuminator. Centrifugations were performed with a VWR MicroStar 12® (11 000 rotations/min for 30 min). For bCA-II inhibition assay, the inhibitory activity (IC_{50}) was evaluated spectrophotometrically at 25 °C using a SPARK® Tecan apparatus and 96 well microplates (Eppendorf). *p*-Nitrophenyl acetate (PNPA) for biological assays was recrystallized from EtOH prior to use and was stored at -25 °C. For KTGS experiments, incubations were conducted in a dedicated oven in which the temperature was maintained to 37 °C.

Representative procedure for the synthesis of vinyl sulfides 3ah and 17: To a solution of 4-(mercaptomethyl)benzenesulfonamide **1a** (0.29 mmol, 1 equiv.) in dry MeCN (3 mL) under argon atmosphere was added the corresponding 7-ethynyl-2H-chromen-2-one (0.33 mmol, 1.1 equiv.). The flask was protected from light and 1,8-diazabicyclo[5.4.0]undec-7-ene (DBU) (0.09 mmol, 0.3 equiv.) was added. The reaction was stirred at room temperature for 2.5 h. Then, reaction was quenched with water and extracted with EtOAc ($\times 2$). The combined organic layers were washed with brine ($\times 1$), then dried over MgSO_4 and the solvents were removed by vacuum. The crude product was purified firstly by flash-column chromatography (silica gel, DCM/EtOAc as a gradient from 100:0 to 98:2, 95:5 and 90/10, v/v) to provide the desired isomers *Z* and *E* as a mixture. Then, both isomers were separated by RP-HPLC (System E) and fractions were collected and lyophilized to provide the desired compounds. (*CAUTION! Every steps described above were performed under a complete protection from light*)

All other characterization data, original spectra, etc., as well as all computational details, are provided in the Supporting Information.

Acknowledgements

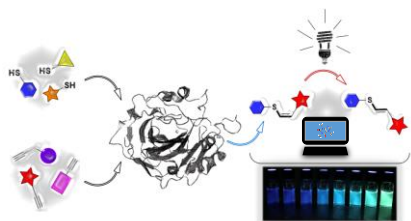
The authors thank the Agence Nationale pour la Recherche (ANR-16-CE07-0004, "Click_and_Fish") for Ph.D fellowship to A.L and the University of Rouen Normandy for Ph.D fellowship to C.P. This work has also been partially supported by University of Rouen Normandy, the Centre National de la Recherche Scientifique (CNRS), INSA Rouen Normandy, European Regional Development Fund (ERDF), Labex SynOrg (ANR-11-LABX-0029), Carnot Institute I2C, the graduate school for research XL-Chem (ANR-18-EURE-0020 XL CHEM), and by Region Normandie. The Centre Régional Informatique et d'Applications Numériques de Normandie (CRIANN) is acknowledged for providing high performance computational resources. Albert Marcual (CNRS) is also acknowledge for HRMS analyses.

Keywords: CA-II • photoisomerization • template synthesis • thiol-yne • vinyl sulfide

- [1] H. Aldewachi, R. N. Al-Zidan, M. T. Conner, M. M. Salman, *Bioengineering (Basel)* **2021**, *8*, 30.
- [2] J. P. Renaud, C. W. Chung, U. H. Danielson, U. Egner, M. Hennig, R. E. Hubbard, H. Nar, *Nat. Rev. Drug. Discov.* **2016**, *15*, 679-698.
- [3] D. Paul, G. Sanap, S. Shenoy, D. Kalyane, K. Kalia, R. K. Tekade, *Drug Discov. Today* **2021**, *26*, 80-93.
- [4] G. Schneider, *Nat. Rev. Drug. Discov.* **2018**, *17*, 97-113.
- [5] a) W. R. Galloway, A. Isidro-Llobet, D. R. Spring, *Nat. Commun.* **2010**, *1*, 80; b) O. C. CJ, H. S. Beckmann, D. R. Spring, *Chem. Soc. Rev.* **2012**, *41*, 4444-4456; c) Y. Shang, C. Wu, Q. Gao, C. Liu, L. Li, X. Zhang, H. G. Cheng, S. Liu, Q. Zhou, *Nat. Commun.* **2021**, *12*, 2988.
- [6] a) E. Oueis, C. Sabot, P. Y. Renard, *Chem. Commun. (Camb)* **2015**, *51*, 12158-12169; b) D. Bosc, J. Jakhilal, B. Deprez, R. Deprez-Poulain, *Future Med. Chem.* **2016**, *8*, 381-404; c) M. Jaegle, E. L. Wong, C. Tauber, E. Nawrotzky, C. Arkona, J. Rademann, *Angew. Chem. Int. Ed.* **2017**, *56*, 7358-7378; d) M. Y. Unver, R. M. Gierse, H. Ritchie, A. K. H. Hirsch, J. *Med. Chem.* **2018**, *61*, 9395-9409; e) D. Bosc, V. Camberlein, R. Gealageas, O. Castillo-Aguilera, B. Deprez, R. Deprez-Poulain, *J. Med. Chem.* **2020**, *63*, 3817-3833.
- [7] Y. Bourne, H. C. Kolb, Z. Radic, K. B. Sharpless, P. Taylor, P. Marchot, *Proc. Natl. Acad. Sci. U S A* **2004**, *101*, 1449-1454.
- [8] N. Willand, M. Desroses, P. Toto, B. Dirie, Z. Lens, V. Villeret, P. Rucktooa, C. Loch, A. Baulard, B. Deprez, *ACS Chem. Biol.* **2010**, *5*, 1007-1013.

- [9] W. G. Lewis, L. G. Green, F. Grynszpan, Z. Radić, P. R. Carlier, P. Taylor, M. G. Finn, K. B. Sharpless, *Angew. Chem. Int. Ed. Engl.* **2002**, *41*, 1053-1057.
- [10] E. L. Wong, E. Nawrotzky, C. Arkona, B. G. Kim, S. Belyny, X. Wang, S. Wagner, M. Lisurek, D. Carstanjen, J. Rademann, *Nat. Commun.* **2019**, *10*, 66.
- [11] M. Jaegle, T. Steinmetzer, J. Rademann, *Angew. Chem. Int. Ed. Engl.* **2017**, *56*, 3718-3722.
- [12] C. Tauber, R. Wamser, C. Arkona, M. Tugend, U. B. Abdul Aziz, S. Pach, R. Schulz, D. Jochmans, G. Wolber, J. Neyts, J. Rademann, *Angew. Chem. Int. Ed. Engl.* **2021**, *60*, 13294-13301.
- [13] F. Mancini, M. Y. Unver, W. A. M. Elgaher, V. R. Jumde, A. Alhayek, P. Lukat, J. Herrmann, M. D. Witte, M. Kock, W. Blankenfeldt, R. Muller, A. K. H. Hirsch, *Chem. Eur. J.* **2020**, *26*, 14585-14593.
- [14] A. Lossouarn, P. Y. Renard, C. Sabot, *Bioconjugate Chem.* **2021**, *32*, 63-72.
- [15] a) R. Masuda, Y. Kawasaki, K. Igawa, Y. Manabe, H. Fujii, N. Kato, K. Tomooka, J. Ohkanda, *Chem. Asian. J.* **2020**, *15*, 742-747; b) A. J. Angelbello, M. D. Disney, *ACS Chem. Biol.* **2020**, *15*, 1820-1825.
- [16] H. Bader, L. C. Cross, I. Heilbron, E. R. H. Jones, *J. Chem. Soc.* **1949**, 619-623.
- [17] J. C. Worch, C. J. Stubbs, M. J. Price, A. P. Dove, *Chem. Rev.* **2021**, *121*, 6744-6776.
- [18] a) R. Castarlenas, A. Di Giuseppe, J. J. Perez-Torrente, L. A. Oro, *Angew. Chem. Int. Ed. Engl.* **2013**, *52*, 211-222; b) N. V. Orlov, *ChemistryOpen* **2015**, *4*, 682-697.
- [19] a) R. Hoogenboom, *Angew. Chem. Int. Ed. Engl.* **2010**, *49*, 3415-3417; b) C. E. Hoyle, A. B. Lowe, C. N. Bowman, *Chem. Soc. Rev.* **2010**, *39*, 1355-1387.
- [20] a) A. B. Lowe, *Polymer* **2014**, *55*, 5517-5549; b) V. X. Truong, A. P. Dove, *Angew. Chem. Int. Ed. Engl.* **2013**, *52*, 4132-4136; c) A. B. Lowe, C. E. Hoyle, C. N. Bowman, *J. Mater. Chem.* **2010**, *20*, 4745-4750.
- [21] a) R. Ekkebus, S. I. van Kasteren, Y. Kulathu, A. Scholten, I. Berlin, P. P. Geurink, A. de Jong, S. Goerdayal, J. Neefjes, A. J. Heck, D. Komander, H. Ovaa, *J. Am. Chem. Soc.* **2013**, *135*, 2867-2870; b) E. Mons, I. D. C. Jansen, J. Loboda, B. R. van Doodewaerd, J. Hermans, M. Verdoes, C. A. A. van Boeckel, P. A. van Veelen, B. Turk, D. Turk, H. Ovaa, *J. Am. Chem. Soc.* **2019**, *141*, 3507-3514.
- [22] S. Sommer, N. D. Weikart, U. Linne, H. D. Mootz, *Bioorg. Med. Chem.* **2013**, *21*, 2511-2517.
- [23] V. Alterio, A. Di Fiore, K. D'Ambrosio, C. T. Supuran, G. De Simone, *Chem. Rev.* **2012**, *112*, 4421-4468.
- [24] a) G. Provensi, F. Carta, A. Nocentini, C. T. Supuran, F. Casamenti, M. B. Passani, S. Fossati, *Int. J. Mol. Sci.* **2019**, *20*, 4724; b) A. Pollard, F. Shephard, J. Freed, S. Liddell, L. Chakrabarti, *Aging (Albany NY)* **2016**, *8*, 2425-2436; c) M. E. Solesio, P. M. Peixoto, L. Debure, S. M. Madamba, M. J. de Leon, T. Wisniewski, E. V. Pavlov, S. Fossati, *Aging Cell* **2018**, *17*, e12787; d) S. Fossati, P. Giannoni, M. E. Solesio, S. L. Cocklin, E. Cabrera, J. Ghiso, A. Rostagno, *Neurobiol. Dis.* **2016**, *86*, 29-40.
- [25] C. B. Mishra, S. Kumari, A. Angeli, S. M. Monti, M. Buonanno, M. Tiwari, C. T. Supuran, *J. Med. Chem.* **2017**, *60*, 2456-2469.
- [26] a) Y. Pocker, J. T. Stone, *Biochemistry* **1967**, *6*, 668-678; b) M. Cauwel, C. Guillou, K. Renault, D. Schapman, M. Benard, L. Galas, P. Cosette, P. Y. Renard, C. Sabot, *Chem. Commun. (Camb)* **2021**, *57*, 3893-3896.
- [27] V. Flon, M. Bénard, D. Schapman, L. Galas, P.-Y. Renard, C. Sabot, *Biomolecules* **2020**, *10*, 619.
- [28] S. S. Matikonda, J. Ivanic, M. Gomez, G. Hammersley, M. J. Schnermann, *Chem. Sci.* **2020**, *11*, 7302-7307.
- [29] A. B. Ghisaidoobe, S. J. Chung, *Int. J. Mol. Sci.* **2014**, *15*, 22518-22538.
- [30] a) H. J. Kang, J. H. Kim, S. J. Chung, *Biosens. Bioelectron.* **2015**, *67*, 413-418; b) J. H. Kim, J. Sumranjit, H. J. Kang, S. J. Chung, *Mol. Biosyst.* **2014**, *10*, 30-33.
- [31] M. M. Lee, B. R. Peterson, *ACS Omega* **2016**, *1*, 1266-1276.
- [32] A. Garg, D. M. Manidhar, M. Gokara, C. Mallela, C. Suresh Reddy, R. Subramanyam, *PLoS One* **2013**, *8*, e63805.
- [33] a) Z. L. Pianowski, *Chem. Eur. J.* **2019**, *25*, 5128-5144; b) A. A. Beharry, G. A. Woolley, *Chem. Soc. Rev.* **2011**, *40*, 4422-4437; c) W. Szymanski, J. M. Beierle, H. A. Kistemaker, W. A. Velema, B. L. Feringa, *Chem. Rev.* **2013**, *113*, 6114-6178; d) W. A. Velema, W. Szymanski, B. L. Feringa, *J. Am. Chem. Soc.* **2014**, *136*, 2178-2191; e) M. Zhu, H. Zhou, *Org. Biomol. Chem.* **2018**, *16*, 8434-8445.
- [34] T. Senthilkumar, L. Zhou, Q. Gu, L. Liu, F. Lv, S. Wang, *Angew. Chem. Int. Ed. Engl.* **2018**, *57*, 13114-13119.
- [35] S. P. Laptinok, A. A. Gil, C. R. Hall, A. Lukacs, J. N. Iuliano, G. A. Jones, G. M. Greetham, P. Donaldson, A. Miyawaki, P. J. Tonge, S. R. Meech, *Nat. Chem.* **2018**, *10*, 845-852.
- [36] I. N. Lee, O. Dobre, D. Richards, C. Ballestrom, J. M. Curran, J. A. Hunt, S. M. Richardson, J. Swift, L. S. Wong, *ACS Appl Mater Interfaces* **2018**, *10*, 7765-7776.
- [37] H. M. Bandara, S. C. Burdette, *Chem. Soc. Rev.* **2012**, *41*, 1809-1825.
- [38] D. H. Waldeck, *Chem. Rev.* **1991**, *91*, 415-436.
- [39] M. Irie, T. Fukaminato, K. Matsuda, S. Kobatake, *Chem. Rev.* **2014**, *114*, 12174-12277.
- [40] R. Klajn, *Chem. Soc. Rev.* **2014**, *43*, 148-184.
- [41] B. Shao, M. Baroncini, H. Qian, L. Bussotti, M. Di Donato, A. Credi, I. Aprahamian, *J. Am. Chem. Soc.* **2018**, *140*, 12323-12327.
- [42] M. W. H. Hoorens, M. Medved, A. D. Laurent, M. Di Donato, S. Fanetti, L. Slappendel, M. Hilbers, B. L. Feringa, W. Jan Buma, W. Szymanski, *Nat. Commun.* **2019**, *10*, 2390.
- [43] a) V. Voliani, R. Bizzarri, R. Nifosi, S. Abbruzzetti, E. Grandi, C. Viappiani, F. Beltram, *J. Phys. Chem. B* **2008**, *112*, 10714-10722; b) S. Mishra, P. Awasthi, J. Singh, R. K. Gupta, V. Singh, R. Kant, R. Jeet, D. Goswami, A. Goel, *J. Org. Chem.* **2018**, *83*, 3669-3678; c) R. Kashihara, M. Morimoto, S. Ito, H. Miyasaka, M. Irie, *J. Am. Chem. Soc.* **2017**, *139*, 16498-16501; d) K. Mutoh, N. Miyashita, K. Arai, J. Abe, *J. Am. Chem. Soc.* **2019**, *141*, 5650-5654; e) Y. Xie, M. C. Arno, J. T. Husband, M. Torrent-Sucarrat, R. K. O'Reilly, *Nat. Commun.* **2020**, *11*, 2460.
- [44] a) J. A. Richard, M. Massonneau, P. Y. Renard, A. Romieu, *Org. Lett.* **2008**, *10*, 4175-4178; b) A. Gandioso, R. Bresoli-Obach, A. Nin-Hill, M. Bosch, M. Palau, A. Galindo, S. Contreras, A. Rovira, C. Rovira, S. Nonell, V. Marchan, *J. Org. Chem.* **2018**, *83*, 1185-1195; c) H. Turki, S. Abid, R. El Gharbi, S. Fery-Forgues, *C. R. Chim.* **2006**, *9*, 1252-1259; d) B. Roubinet, A. Chevalier, P.-Y. Renard, A. Romieu, *Eur. J. Org. Chem.* **2015**, *2015*, 166-182; e) B. Roubinet, C. Massif, M. Moreau, F. Boschetti, G. Ulrich, R. Ziessel, P. Y. Renard, A. Romieu, *Chem. Eur. J.* **2015**, *21*, 14589-14601; f) M. Y. Wu, K. Li, C. Y. Li, J. T. Hou, X. Q. Yu, *Chem. Commun. (Camb)* **2014**, *50*, 183-185; g) B. Roubinet, P.-Y. Renard, A. Romieu, *Dyes Pigm.* **2014**, *110*, 270-284; h) M. Bojtar, K. Nemeth, F. Domahidy, G. Knorr, A. Verkman, M. Kallay, P. Kele, *J. Am. Chem. Soc.* **2020**, *142*, 15164-15171.
- [45] a) N. Holzmann, L. Bernasconi, R. H. Bisby, A. W. Parker, *Phys. Chem. Chem. Phys.* **2018**, *20*, 27778-27790; b) T. Nakamura, S. Takeuchi, T. Taketsugu, T. Tahara, *Phys. Chem. Chem. Phys.* **2012**, *14*, 6225-6232.

Metalloenzyme-Mediated Thiol-Yne Addition towards Photoisomerizable Fluorescent Dyes



A regioselective metalloenzyme-directed synthesis of a vinyl sulfide-based inhibitor, which has shown to be involved in an unexpected *Z* to *E* photoisomerization process, is reported. Tuning of the spectral features guided by theoretical studies, revealed structural modifications for effective bidirectional photoconversion of thermally bistable vinyl sulfide diastereoisomers, while maintaining high the biological activity of the parent inhibitor.